Optical to UV spectra and birefringence of SiO_2 and TiO_2: First-principles calculations with excitonic effects

H. M. Lawler,[1] J. J. Rehr,[1] F. Vila,[1] S. D. Dalosto,[1,2] E. L. Shirley,[2] and Z. H. Levine[2]
[1]*Department of Physics, University of Washington, Seattle, Washington 98195, USA*
[2]*National Institute of Standards and Technology, Gaithersburg, Maryland 20899, USA*
(Received 11 July 2008; revised manuscript received 13 October 2008; published 12 November 2008)

A first-principles approach is presented for calculations of optical, ultraviolet spectra including excitonic effects. The approach is based on Bethe-Salpeter equation calculations using the NBSE code combined with ground-state density-functional theory calculations from the electronic structure code ABINIT. Test calculations for bulk Si are presented, and the approach is illustrated with calculations of the optical spectra and birefringence of α-phase SiO_2 and the rutile and anatase phases of TiO_2. An interpretation of the strong birefringence in TiO_2 is presented.

DOI: 10.1103/PhysRevB.78.205108 PACS number(s): 78.20.Bh, 78.20.Fm, 78.20.Ci, 71.35.−y

I. INTRODUCTION

As in many subfields in condensed matter physics, the application of density-functional theory (DFT)[1–3] has significantly influenced studies of material optical properties. However, treatments based on Kohn-Sham dipole transitions alone only provide a beginning for modeling optical spectra since a ground-state one-electron approach cannot account for a range of excited-state and optical effects. Thus, quantitative calculations of optical spectra require the integration of DFT with a number of many-body techniques. Local field corrections from the random phase approximation (RPA) alone are inadequate to reproduce near-gap optical spectra because they do not take into account self-energy and excitonic effects. Consequently a quantitative theory and interpretation must also include quasiparticle self-energy effects based, e.g., on the *GW* method,[4,5] and particle-hole interactions based on the Bethe-Salpeter equation (BSE).[6] The success of the BSE method has effectively settled the long-running discussion of the origin of many low-energy spectral features.[7,8] For example, for the rutile phase of TiO_2, early studies could only speculate about the relative importance of excitonic effects versus band-structure topology in the dominant threshold absorption,[9] whereas we show here that these features are dominated by excitonic effects.

While the BSE is often necessary for accurate calculations of optical spectra, the approach has had limited applications largely due to a lack of efficient computational methods for general systems. To address this need, we have developed an approach based on an interface, here dubbed AI2NBSE, between the BSE code NBSE (NIST Bethe-Salpeter equation) developed at National Institute of Standards and Technology (NIST)[10] and the general purpose DFT electronic structure code ABINIT.[11] One of the objectives of this work is to improve the availability of BSE codes. Our interface also provides a comparison to the BSE codes EXC (Ref. 12) and EXC!TING,[13] and other recent codes,[14] and also to approaches which model electron-hole interactions within time-dependent density-functional theory (TDDFT).[15] The latter calculations are usually simpler than BSE ones, but in practice are limited by an incomplete knowledge of the exchange-correlation functional and the neglect of damping effects. The overall strategy of our interface also differs from EXC in several respects, although both make use of ABINIT. For example our AI2NBSE interface achieves efficiency in the BSE calculations through the use of the Hybertsen-Levine-Louie[16,17] dielectric screening, and can also treat finite momentum transfer. Also, the interface requires only generic input, and, thus, can be adapted to other ground-state and BSE codes.

The interface is tested on bulk Si, yielding results in good agreement with other approaches. In particular we find that the calculations based on ABINIT are in excellent agreement with those from the optimal basis function (OBF) code.[18] As initial applications, we report optical spectra and anisotropic optical properties of the common rutile and anatase phases of TiO_2, and for the α-quartz phase of SiO_2. These are important materials for many applications.[19,20] However, we are not aware of earlier calculations for TiO_2 that include electron-hole interactions, which are needed to reproduce their rich dependence on polarization and phase.

In the remainder of this paper we briefly summarize the key formulas describing excitonic effects and other features of NBSE. We then briefly describe our integration of ABINIT and NBSE, using bulk Si as an illustrative test case, with some further details in the Appendix. Finally, calculations are presented for the birefringent spectra of α quartz, and similarly for the rutile and anatase phases of TiO_2, followed by a summary and conclusions.

II. BSE AND EXCITONIC EFFECTS

A. Exciton secular equation

In this paper we briefly summarize the BSE formalism, following the notation and theoretical developments of Shirley *et al.*[21] Formally the BSE provides a complete theory for optical spectra through a hierarchy of equations derived from the two-particle Green's function.[22,23] However, with certain approximations to the electron-hole interaction, the BSE can be reduced to an eigenvalue problem of an effective particle-hole Hamiltonian[24]

$$H|f\rangle = [H_{1e} + H_{2e}]|f\rangle = \Omega_f|f\rangle, \tag{1}$$

where the eigenstates $|f\rangle$ are given by a superposition of particle-hole basis states[25] $|nn'\mathbf{k}(\mathbf{q})\rangle$, i.e.,

$$|f\rangle = \sum_{nn'\mathbf{k}} \psi_f[nn'\mathbf{k}(\mathbf{q})]|nn'\mathbf{k}(\mathbf{q})\rangle,$$

$$|nn'\mathbf{k}(\mathbf{q})\rangle \equiv a_{n\mathbf{k}}a^{\dagger}_{n'\mathbf{k}+q}|0\rangle, \tag{2}$$

and throughout this paper we use atomic units ($e=\hbar=m=1$). Here $\psi_f[nn'\mathbf{k}(\mathbf{q})]$ is the amplitude of a given particle-hole (or excitonic) state with Bloch crystal momentum index $\mathbf{k}$ and momentum transfer $\mathbf{q}$, the index n runs over all occupied valence bands, the index n' runs over unoccupied bands, and $|0\rangle$ denotes the many-body ground-state with energy $\Omega_0=0$. For optical absorption $\mathbf{q}$ is usually negligible. However for inelastic x-ray scattering and other spectroscopies and for computational purposes, it is desirable to retain the explicit momentum-transfer dependence. The single-particle contribution to the Hamiltonian for a particle-hole pair is diagonal in the quasiparticle or quasihole basis so that one has

$$H_{1e}|nn'\mathbf{k}(\mathbf{q})\rangle = (E_{n'\mathbf{k}+\mathbf{q}} - E_{n\mathbf{k}})|nn'\mathbf{k}(\mathbf{q})\rangle, \tag{3}$$

where the quasiparticle energies $E_{n\mathbf{k}}$ are Kohn-Sham eigenvalues $\varepsilon_{n\mathbf{k}}$ plus quasiparticle self-energy corrections

$$E_{n\mathbf{k}} = \varepsilon_{n\mathbf{k}} + \Sigma_{n\mathbf{k}}. \tag{4}$$

Here $\Sigma_{n\mathbf{k}}$ is the self-energy calculated in the *GW* approximation for which efficient approximations have been developed.[21,26]

The electron-hole interaction contribution includes both "direct" and "exchange" couplings $H_{2e}=V_D+V_X$,

$$H_{2e}|nn'\mathbf{k}(\mathbf{q})\rangle = \sum_{n''n'''\mathbf{k}} [V_D(nn'\mathbf{k},n''n'''\mathbf{k}';\mathbf{q}) + V_X(nn'\mathbf{k},n''n'''\mathbf{k}';\mathbf{q})]|n''n'''\mathbf{k}'(\mathbf{q})\rangle, \tag{5}$$

with matrix elements defined explicitly below. Once the BSE secular equation is solved, the optical constants may be obtained formally using a Fermi golden rule expression in terms of the excitonic final states coupled to the currentlike operator J'_μ. In the NBSE code, however, these properties are calculated using resolvent techniques. In particular the imaginary part of the dielectric tensor is given in terms of resolvents

$$\mathrm{Im}\ \epsilon_{\mu\nu}(\omega) = -4\pi\ \mathrm{Im}[\langle 0|J'_\mu[\omega - H + i\eta]^{-1}J'_\nu|0\rangle - \langle 0|J'_\nu[-\omega - H - i\eta]^{-1}J'_\mu|0\rangle]. \tag{6}$$

In terms of the particle-hole states, the currentlike operator coupling to the ground state is given approximately by

$$J'_\mu|0\rangle \approx \sum_{nn'\mathbf{k}} |nn'\mathbf{k}(\mathbf{q})\rangle \frac{\langle\psi_{n'\mathbf{k}+\mathbf{q}}|J_\mu|\psi_{n\mathbf{k}}\rangle}{\varepsilon_{n'\mathbf{k}+\mathbf{q}} - \varepsilon_{n\mathbf{k}}}, \tag{7}$$

where J_μ is the μth component of the current operator and $\psi_{n\mathbf{k}}$ are approximated as Kohn-Sham one-particle states. For small q, the matrix elements of J_μ are approximated by

$$\frac{1}{\omega}\langle\psi_{n'\mathbf{k}+\mathbf{q}}|J_\mu|\psi_{n\mathbf{k}}\rangle \approx \left(\frac{\varepsilon_{n'\mathbf{k}+\mathbf{q}} - \varepsilon_{n\mathbf{k}}}{\omega q_\mu}\right)\langle\psi_{n'\mathbf{k}+\mathbf{q}}|e^{i\mathbf{q}\cdot\mathbf{r}}|\psi_{n\mathbf{k}}\rangle \approx \frac{1}{q_\mu}\langle\psi_{n'\mathbf{k}+\mathbf{q}}|e^{i\mathbf{q}\cdot\mathbf{r}}|\psi_{n\mathbf{k}}\rangle, \tag{8}$$

where $\mathbf{q}=q\hat{\mu}$. In the NBSE code these resolvents in the above expressions for the dielectric tensor are calculated using an efficient iterative Lanczos algorithm.[27]

B. Electron-hole Interaction

The interaction kernel H_{2e} of Eq. (5) accounts for two processes, which scatter an electron from band n' to band n''', and a hole from band n to band n''. The first is the attractive direct screened Coulomb interaction between the electron and the hole, and the second is the repulsive unscreened exchange interaction. Each of these contributions can be written in terms of two-particle integrals between electron and hole Kohn-Sham orbitals $\psi_{n\mathbf{k}}(\mathbf{x})$ and $\psi_{n'\mathbf{k}+\mathbf{q}}(\mathbf{x})$. Matrix elements of the direct term are given by

$$V_D(nn'\mathbf{k},n''n'''\mathbf{k}';\mathbf{q}) \approx -\int d^3x\,\psi^*_{n'''\mathbf{k}'+\mathbf{q}}(\mathbf{x})\psi_{n'\mathbf{k}+\mathbf{q}}(\mathbf{x})\int d^3x'\,\psi^*_{n\mathbf{k}}(\mathbf{x}') \times \psi_{n''\mathbf{k}'}(\mathbf{x}')W(\mathbf{x},\mathbf{x}';\omega=0). \tag{9}$$

Here the electron-hole interaction $W(\mathbf{x},\mathbf{x}';\omega)$ is the screened Coulomb attraction as mentioned above, i.e., $W=\epsilon^{-1}(\omega)V$, which in an exact theory should include the frequency dependence of the dielectric response. However the NBSE code approximates the screening with the static, spatially dependent Hybertsen-Levine-Louie dielectric function.[16,17] This model maps the local density in real solids to the density dependence in a homogeneous system. These calculations require the ground-state density, whose Fourier coefficients are

$$\rho(\mathbf{G}) = \frac{2}{N}\sum_{n\mathbf{k},\mathbf{G}'} f_{n\mathbf{k}}\psi_{n\mathbf{k}}(\mathbf{G}+\mathbf{G}')\psi^*_{n\mathbf{k}}(\mathbf{G}'), \tag{10}$$

where $f_{n\mathbf{k}}=\theta(\varepsilon_F-\varepsilon_{n\mathbf{k}})$ is the occupation of state $n\mathbf{k}$, N is the number of unit cells in the ABINIT calculation, which is the same as the number of $\mathbf{k}$ points in the calculation, and spin degeneracy is assumed. Here $\psi_{n\mathbf{k}}(\mathbf{G})$ are the Fourier coefficients of the Bloch wave expansion[17] in reciprocal lattice vectors

$$\psi_{n\mathbf{k}}(\mathbf{x}) = e^{i\mathbf{k}\cdot\mathbf{x}}\sum_{\mathbf{G}} \psi_{n\mathbf{k}}(\mathbf{G})e^{i\mathbf{G}\cdot\mathbf{x}}. \tag{11}$$

Because the dielectric function is modeled locally, the exciton amplitudes must be transformed from the Bloch basis to a local basis with coordinates $\mathbf{x}$ and $\mathbf{x}'$. These local coordinates can be considered as transform analogs of the band and wave-vector indices n, n', and $\mathbf{k}$.[10]

Similarly matrix elements of the exchange term are

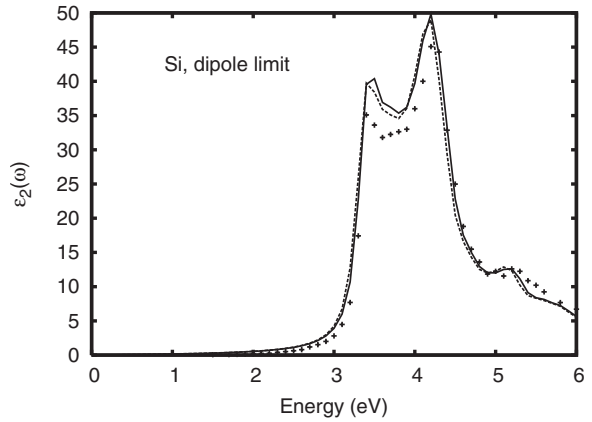

FIG. 1. Imaginary part of the dielectric function for Si using NBSE and two different ground-state inputs; one set of inputs is from OBF (dashed line) and the other from ABINIT (solid line). For comparison the experimental spectrum is also plotted (crosses).

$$V_X(nn'\mathbf{k},n''n'''\mathbf{k}';\mathbf{q}) \approx +2\int d^3x \psi^*_{n'''\mathbf{k}'+\mathbf{q}}(\mathbf{x})\psi_{n''\mathbf{k}'}(\mathbf{x}) \times \int d^3x' \psi^*_{n\mathbf{k}}(\mathbf{x}')\psi_{n'\mathbf{k}+\mathbf{q}}(\mathbf{x}')\frac{1}{|\mathbf{x}-\mathbf{x}'|}. \quad (12)$$

As noted, for example by Hybertsen and Louie, the exchange term in the BSE should be unscreened.

The matrix dimension of the electron-hole interaction H_{2e} is generally very large. For example, for the calculations for SiO_2 presented below, 216 **k** points are sampled, and there are 24 doubly-degenerate valence (hole) states and 26 conduction (electron) states. For this case, there are over 10^5 electron-hole pairs, each requiring a representation in both periodic and local bases.

C. AI2NBSE interface

The above theory has been implemented in a modular code, which uses the output of ground-state density-functional theory calculations from the electronic structure code ABINIT as input to Bethe-Salpeter equation calculations using the NBSE code. The interface serves as a driver for both ABINIT and NBSE, starting from a single input file, and also constructs the various physical quantities and arrays needed in the calculations. No explicit changes in the structure or coding of either ABINIT or NBSE are used. Both the interface and documentation are available from the authors.[28] Additional details are given in Appendix.

III. OPTICAL SPECTRA OF SILICON

As a quantitative test, illustrative results from AI2NBSE for bulk Si are presented in Fig. 1. The two spectra compared are each calculations of the imaginary part of the dielectric function for bulk Si using NBSE: in one case the ground-state quantities above are calculated with the OBF pseudopotential, plane-wave code[18]—for which NBSE was originally designed—and in the other case the same quantities are calculated from ABINIT. In both calculations 20 valence and conduction bands were included with an eight Hartree cutoff criteria for the vectors **G**. The close quantitative agreement between OBF and ABINIT, thus, serve as a quality check on the various theoretical and algorithmic approximations used in our interface.

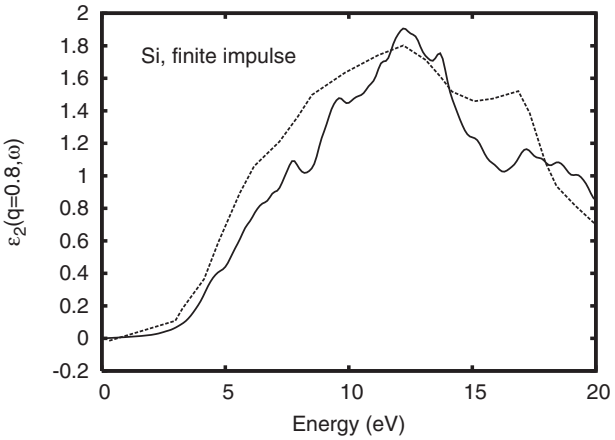

FIG. 2. Calculated $\varepsilon_2(\mathbf{q},\omega)$ for Si with impulse magnitude of $q=0.8\ a_0^{-1}$ along the [1,1,1] direction. AI2NBSE's result (solid line), and for comparison the result from a recent TDDFT calculation (dashed line) are plotted (Ref. 29).

Our AI2NBSE interface can also be applied to finite momentum-transfer calculations. For example, Fig. 2 illustrates the spectrum for a momentum transfer of magnitude $q=0.8\ a_0^{-1}$, where a_0 is the Bohr radius. Results from a recent TDDFT calculation are also plotted.[29]

IV. OPTICAL SPECTRA OF α QUARTZ

The excitonic character of the α-quartz optical spectra had been recognized even before first-principles investigations became possible.[30,31] The large band gap and small static dielectric constant of α quartz, and the prominent low-energy features in the spectrum, suggest a strong excitonic role in the optical properties, which was subsequently confirmed by first-principles calculations.[25] Our calculations, like those of Ref. 25, reproduce the measured spectra in detail, with excellent agreement in oscillator strength and calculated feature positions corresponding with those measured to within tenths of an eV. The results can be seen in Fig. 3.

The calculations of Ref. 25 were performed for photon polarization within the hexagonal plane (i.e., the "ordinary ray"), noting that this is the most commonly measured spectrum. However, this material is uniaxial, possessing an independent optic axis normal to the hexagonal plane. We have also carried out calculations for photon polarization perpendicular to the hexagonal plane (i.e., the "extraordinary ray"). As illustrated in Fig. 3, α quartz exhibits some anisotropy, but it is less pronounced than for rutile. This result is consistent with the known role of the SiO_4 tetrahedron versus the anisotropic crystal structure, and the structural phase insensitivity of the optical functions in quartz.[30]

While birefringence in α quartz is a well-studied effect, it is small relative to TiO_2 crystals discussed in Sec. V. Below

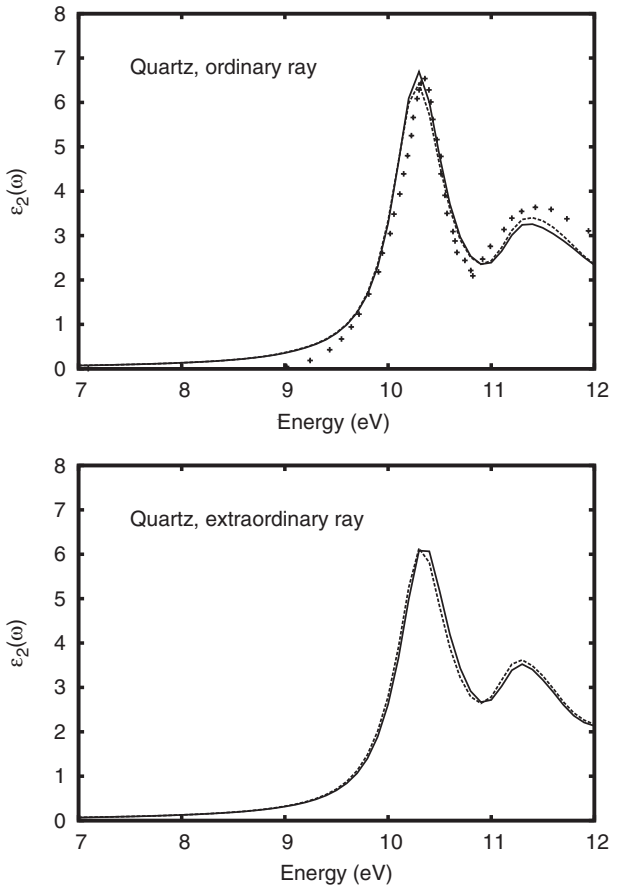

FIG. 3. Imaginary part of the dielectric function for SiO_2 with in-plane polarization (top), and out-of-plane polarization (bottom). Theoretical spectra from ABINIT and OBF (solid line and dashed line) spectra are plotted for both polarizations. The calculated spectra use a 28 Hartree plane-wave cutoff and included a 216 **k**-point Brillouin zone sampling and the 26 lowest-lying degenerate bands above the Fermi level. The experimental spectrum, reproduced from Ref. 25, is also shown (crosses) for the ordinary ray.

the interband transition energies, but above the lattice response, we find static indices of refraction of 1.52 for the ordinary polarization, and 1.53 for the extraordinary at 0.7 eV, in precise agreement with the measured values.[32]

V. OPTICAL SPECTRA OF RUTILE AND ANATASE

As one of the simplest transition-metal oxides, TiO_2 exhibits a variety of natural crystal structures and presents a fundamentally interesting system for first-principles electronic structure methods. This material is also an important component in various ultraviolet (UV) applications. It has been demonstrated that *ab initio* methods can describe various physical properties of TiO_2.[19,20] There have been a few *ab initio* studies of UV dielectric spectra for rutile and anatase phases. Glassford and Chelikowsky[33] reported calculations for the rutile phase using a plane-wave pseudopotential approach; Mo and Ching[34] used a linear-combination-of-atomic-orbital method for both phases (and brookite); and Asahi *et al.*[35] studied the anatase phase with a linearized

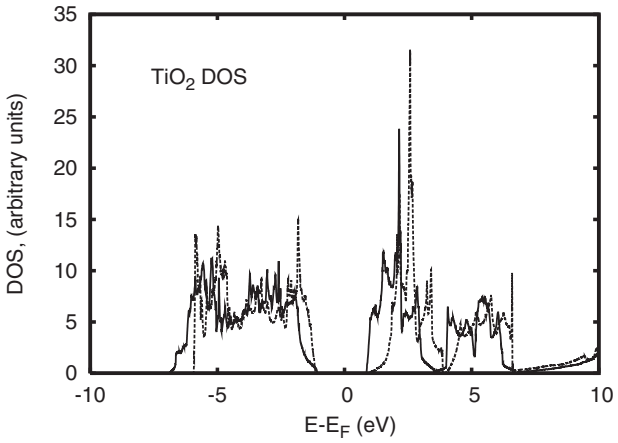

FIG. 4. Density of states $\rho(E)$ with respect to the Fermi energy E_F for the uppermost valence and lowest conduction bands of TiO_2 in the rutile (solid line) and anatase (dashed line) phases. No band-gap corrections are included. The LDA gap is calculated to be 2.0 eV for rutile and 2.2 eV for anatase.

augmented plane-wave method. However, none of these studies included excitonic effects. A theoretical treatment that includes excitonic states may contribute to understanding its optical properties. Toward this end, we present calculations of the spectra of TiO_2, with polarization dependence, for both the rutile and anatase phases using our AI2NBSE interface.

Each of the two TiO_2 phases is tetragonal, and Mo and Ching[34] and Fahmi *et al.*[36] reviewed their structural properties including crystal structures, space groups, and differences in bond lengths and angles. These two crystal structures can be considered as arrangements of slightly distorted oxygen octahedral elements with a titanium atom at the center of each so that each titanium has an oxygen coordination of six and each oxygen has a titanium coordination of three. The relationship between the two structures has been described in terms of varied orientation among the octahedral chains. The two polymorphs studied here can be generated with six-atom unit cells corresponding to two TiO_2 units. Each unit possesses two inequivalent bonds of "apical" and "equatorial" character, such that each titanium atom sees two apical and four equatorial bonds, while each oxygen atom sees one apical and two equatorial bonds.

Structural similarities in rutile and anatase lead to similarities in their electronic structure. In Fig. 4 we plot the ABINIT-calculated densities of states for the two materials. The local-density approximation (LDA) gives the uppermost valence-band width of about 5 eV for anatase and 6 eV for rutile, and this band is regarded to be dominated by O $2p$ character. The anatase LDA band gap is greater than that of rutile by about 0.2 eV, corresponding with the measured difference.[37] Because the oxygen-bonding environment is planar in both phases, there is a decomposition of the O $2p$ into p_π and p_σ states.[35,38] The first conduction band is dominated by Ti $3d$ character, with the lower half regarded as t_{2g} like, and the upper half regarded as e_g like.[35,38] As can be seen in Fig. 4 and from the band structures,[19] these subbands are reasonably resolved energetically.

We performed calculations with semicore states treated as core using Troullier-Martins-type pseudopotentials,[33,39] and

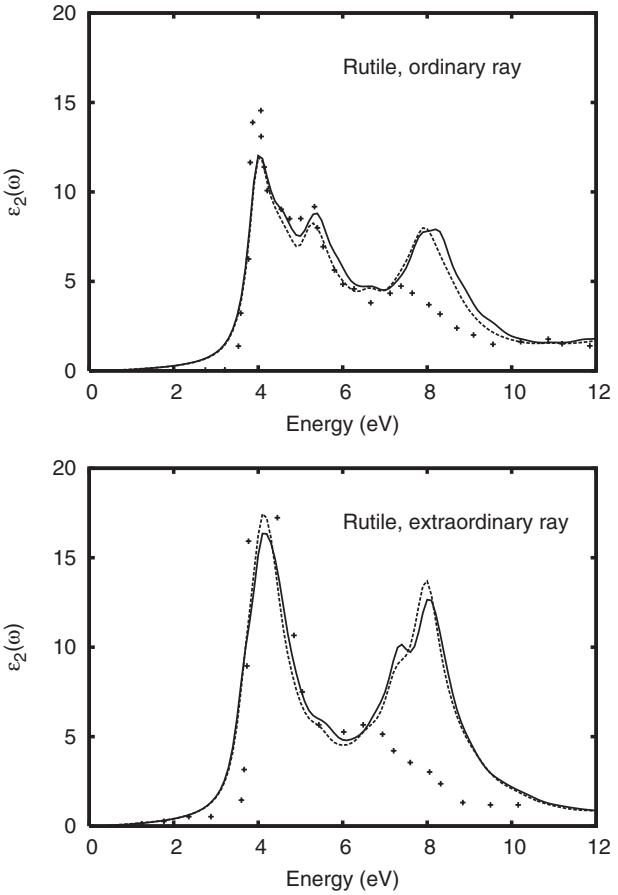

FIG. 5. Imaginary part of the dielectric function for rutile with in-plane polarization (top) and out-of-plane polarization (bottom). Theoretical from ABINIT and OBF (solid line and dashed line) spectra are plotted for both polarizations. The calculated spectra use a 32 Hartree plane-wave cutoff and included a 216 **k**-point Brillouin zone sampling and the 26 lowest-lying degenerate bands above the Fermi level. For comparison the experimental spectrum from Ref. 9 (crosses) is also plotted.

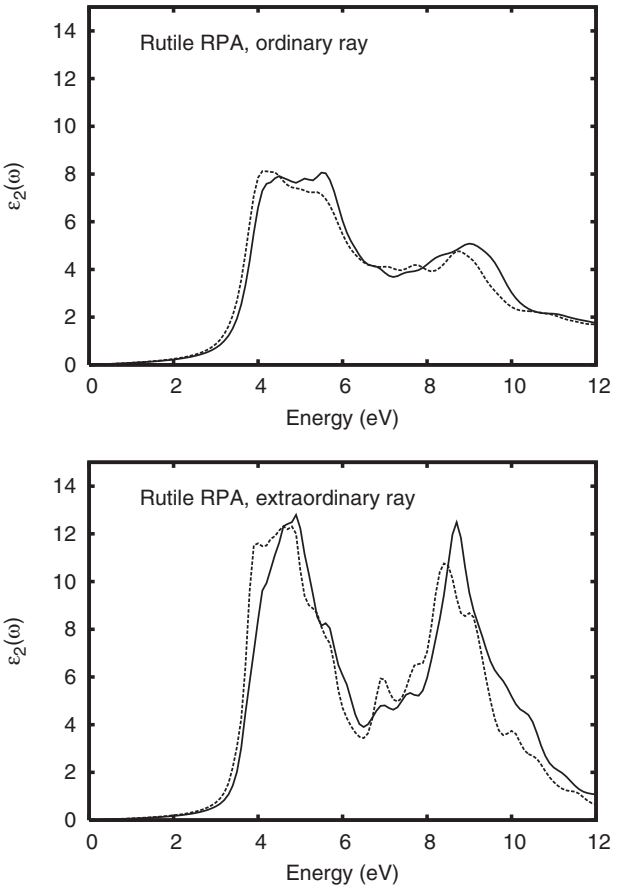

FIG. 6. Imaginary part of the dielectric function for rutile with in-plane polarization (top) and out-of-plane polarization (bottom) calculated without core-hole interactions (V_D=0). Two spectra are plotted corresponding to a treatment of semicore states with Teter-type Ti pseudopotentials (solid line), and with Troullier-Martins pseudopotentials where the semicore states are pseudized (dashed line).

as valence using Teter-type pseudopotentials.[19,40] While the semicore states have spatial localizations comparable to oxygen 2*p* states, their energies are many eV below the Fermi level. Our calculations suggest that the optical and UV spectra are not highly sensitive to the treatment of Ti semicore states, and that the primary source of the discrepancy between theoretical and experimental spectra is the neglect of the excitonic effects in the low-energy region.

A. Rutile phase

The spectra calculated for rutile with the AI2NBSE interface (Fig. 5) demonstrate significant excitonic effects, as can be seen by comparison with calculations (Fig. 6), which neglect electron-hole interactions and are calculated within the RPA.

One signature of the excitonic effects is the sharp onset in our BSE calculations, which better reproduces experimental spectra. Our results for the polarization dependence in TiO_2 show a much more prominent anisotropic optical response than in SiO_2. This results in strong birefringence, as seen in Fig. 7. Our calculated static indices of refraction differ by 0.30, in agreement with the observed birefringence.[9]

Two pronounced anisotropic features in our calculations are consistent with experimental spectra.[9,41] First, the primary onset absorption feature assumes a doublet structure for the ordinary ray, which is not evident for the extraordinary ray. These low-energy excitonic features at 4.0 and 5.3 eV are clearly evident in our calculation and are expected to involve t_{2g}-like final states.[34] Second, the onset of absorption for the extraordinary ray is significantly stronger than for the ordinary. For the extraordinary ray, a single feature is measured at 4.1 eV, which is stronger, broader, and more symmetric than for the ordinary ray. However, a third anisotropic feature of our calculations, namely, the much stronger absorption peak for the extraordinary ray above 6 eV, is not clearly seen in the experimental reflectivity spectra. To summarize, our BSE calculation gives a stronger, less structured t_{2g}-like absorption band for the extraordinary ray than for the ordinary, in accord with experiment.

Above 7 eV, there is notable discrepancy between the theoretical and experimental rutile spectra. The origin of the prominent absorption above 7 eV has been established as

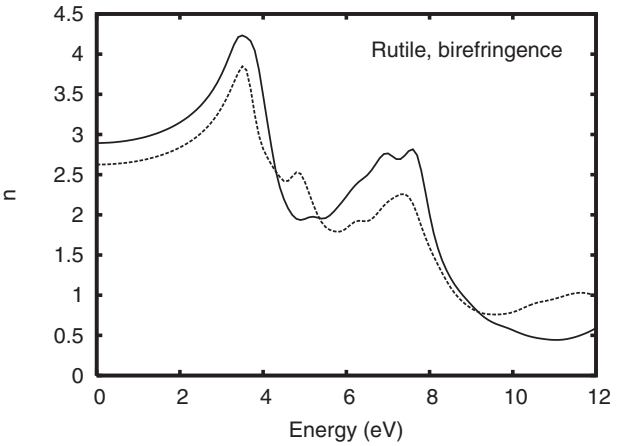

FIG. 7. Ordinary (dashed line) and extraordinary (solid line) indices of refraction n of rutile TiO_2 as a function of photon energy. At 589 nm, which is below the band gap but well above the lattice resonances, the calculated difference between the two indices is 0.30 while the measured value is 0.29 (Ref. 9).

"transitions between the O $2p$ orbitals and the e_g conduction-band states,"[34] an analysis consistent with the present results. However, the bandwidths and centroid separations between the e_g and t_{2g} subbands from the density of states and from the optical spectra agree to within 20%, with differences arising from valence-state dispersion and matrix-element effects.

The data of Cardona and Harbeke[9] are obtained from reflectance measurements and rely on Kramers-Kronig transformations. Overall the spectra of their influential work exhibits smaller absorption above 7 eV than that calculated in available first-principles work or that measured for anatase. Also their data exhibits less prominent e_g features than what appear in the measured x-ray absorption spectra.[33,42] Toward a critical comparison of our calculated spectra and those of Ref. 9, we compared the effective oscillator strength contributions from our calculated absorption with that from the experimental spectrum. If we consider the net oscillator strength in the absorption up to 12 eV, the experimental spectrum gives about seven electrons per primitive cell, while our calculated spectrum gives about eight. Though they agree to within about 10%, both of these numbers are low compared to the net valence-band charge of 24 electrons within a range of 10 eV below the Fermi level, and reflect a relatively slow increase in net oscillator strength with increasing energy for TiO_2. Indeed, by analyzing an additional calculation containing 200 conduction bands, we found that one reaches a net oscillator strength of 24 electrons only at 39 eV. We also found that the net oscillator strength in our calculation saturates at about 44 electrons above about 100 eV, a number comparable to the 48 valence and semicore states of the TiO_2 units included in the pseudopotential calculation. This slow increase in the net oscillator strength is in contrast to that observed in type IV and type III-V cubic materials, where saturation occurs typically within the first 20 eV.[43] The slow increase for TiO_2 is partly due to the forbidden nature of $2s$-$2p$ transitions, which forces a significant amount of oscillator strength to higher energies.

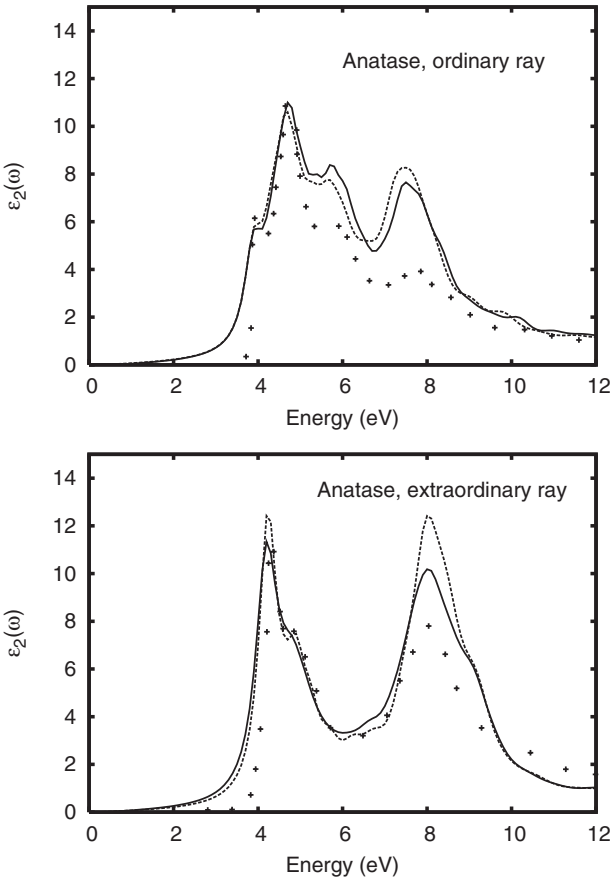

FIG. 8. Imaginary part of the dielectric function for anatase with in-plane polarization (top) and out-of-plane polarization (bottom). Theoretical spectra from ABINIT and OBF (solid and dashed lines) are plotted for both polarizations. The calculated spectra use a 32 Hartree plane-wave cutoff and include a 216 **k**-point Brillouin zone sampling and the 26 lowest-lying degenerate bands above the Fermi level. For comparison the experimental spectrum reproduced from Ref. 9 (crosses) are also plotted.

B. Anatase phase

Theoretically, both the valence-band and conduction-band densities of states are similar to that of rutile, as shown in Fig. 4. However, their experimental absorption spectra show more variation (Fig. 8.). Strikingly, the measured spectrum of anatase for the ordinary ray (in-plane polarized) shows a clear low-energy shoulder below the primary absorption feature.[41,44] This feature is not seen in rutile, and calculations neglecting the electron-hole interactions in anatase do not clearly resolve it.[34,35] Aside from this low-energy feature, the spectral structure and anisotropy of anatase, both calculated and measured, have some similarities to that of rutile. Thus features in the spectra have been analyzed,[35,44] and conclusions regarding the relevant bands are reminiscent of results for rutile.[33] For the e_g-like absorption band, the experimental spectrum for anatase does show a stronger absorption for the extraordinary ray,[44] similar to what is calculated in both the rutile and anatase phases, but not seen in experimental rutile spectrum. We have found, by comparing results from Teter-type and Troullier-Martins pseudopotentials that part of the disagreement at high energy between the ABINIT and OBF

results for the anatase extraordinary ray is due to differences in the pseudopotentials used.

C. Interpretation of polarization dependence

Molecular-orbital interpretations of the TiO_2 spectra have been reported widely[42,45] and provide a qualitative picture of the electronic structure in this system. Such analyses illustrate the hybridization between the Ti $3d$ and O $2p$ states. However, immediately above and below the Fermi level, the hybridization has been shown to be weak.[35,38] The calculations of Sorantin and Schwartz[35] demonstrate that the valence band for rutile just below the Fermi level is primarily π-bonding O $2p$ character, while lower in energy is primarily σ-bonding O $2p$ character. Just above the Fermi level, the states are, in energetic order, primarily Ti t_{2g} and e_g.

A molecular-orbital analysis, considered in conjunction with measured x-ray spectra, allowed an empirical identification of features in the optical spectra of Harbeke and Cardona[9] with specific electronic transitions.[42] Although selection rules, inferred from the approximate atomic states, were invoked in that work, no effort was made to analyze the polarization dependence of the selection rules. Some of the most prominent features could not be identified at all, and were attributed to the unaccounted excitonic effects. Assignments of the same experimental features were made, for ordinary and extraordinary rays independently, from a band-structure perspective by Glassford and Chelikowsky.[33] But the calculated spectra again did not treat the excitonic interactions, and hence, did not reproduce the experimental features to the level of agreement reported here. Also, local electronic structure was not emphasized in the peak assignment analysis.

Perhaps the most conspicuous anisotropic characteristic in the rutile spectra is the stronger onset absorption for the extraordinary ray. We observe that the first eV below the Fermi level is dominated by the O $2p_\pi$ states, and further, that the oxygen-bonding planes are all defined by in-hexagonal-plane normals. This implies that for some in-plane polarization, there is a single dipole-allowed channel from one of the two π-state orientations (corresponding to the two oxygen-bonding planes), and the three t_{2g} states, while for the extraordinary polarization, there are two dipole-allowed channels. This is consistent with the calculated and measured stronger threshold resonance for the extraordinary ray. In connection with this point, we emphasize that while the t_{2g} and e_g symmetry labels are approximate because of angular and bond-length distortions within the octahedra, the selection rules above are unmodified even when the local, D_{2h}, symmetry group is considered, while the actual crystallographic group in rutile is of even higher symmetry.

VI. SUMMARY AND CONCLUSIONS

In summary, we have developed a first-principles approach for calculations of various optical spectra, including finite momentum transfer in crystals. The method combines ground-state electronic structure calculations from ABINIT with BSE calculations from the NBSE code. The method is tested on bulk Si, yielding results in good agreement with other methods. Calculations are presented for the macroscopic dielectric spectra and its orientation dependence in α quartz, rutile TiO_2, and anatase TiO_2. Our quartz spectra for the ordinary ray reproduce the strong excitonic character and are in good agreement with experiment and earlier theoretical work. The anisotropies of the rutile and anatase phases of TiO_2 are more significant than for quartz. The static indices of refraction for the two polarizations of rutile differ by more than 10%, in agreement with experiment. Also our calculated absorption at low energies reproduces experiment better than previous theoretical results that neglect excitonic effects. In particular our calculations reveal an additional low-energy feature in anatase also found in experiment. Also we are able to interpret the anisotropy in the threshold behavior for rutile in terms of π to t_{2g} selection rules.

ACKNOWLEDGMENTS

This work was supported by U.S. DOE under Grant No. DE-FG03-97ER45623 (J.J.R., H.M.L., S.D.D.), by NIST under Grant No. 70 NANB7H6141 (S.D.D.), and was facilitated by the DOE Computational Materials Science Network. M. Prange, J. Kas, and A. Sorini assisted with testing the interface. We also thank L. Reining, V. Olevano, S. Ismail-Beigi, and especially X. Gonze and the ABINIT development group for helpful discussions.

APPENDIX: AI2NBSE INTERFACE

In order to calculate the optical spectra, the AI2NBSE interface first obtains Kohn-Sham energies and wave functions from the self-consistent ground-state electronic structure code ABINIT. The single-particle eigenenergies are modified to include self-energy corrections according to the *GW* approximation. Subsequently the interface constructs several quantities needed for the NBSE calculations. These include current-operator matrix elements between Kohn-Sham states and the ground-state charge density for calculating Hybertsen-Levine-Louie screening. Thus, our interface does not take advantage of ABINIT's dielectric function capability.

Typical AI2NBSE calculations are divided into four modular stages and require a single input file, which contains all parameters needed to define both the system and its ground-state and excited-state one-electron properties. Briefly the modular operations are as follows after the input file is read and stored:

(1) ABINIT *calculation*: ABINIT inputs are generated and ABINIT is run. These calculations supply the Kohn-Sham eigenvalues $\varepsilon_{n\mathbf{k}}$ and eigenfunctions $\psi_{n\mathbf{k}}$ both for the occupied and unoccupied states. Currently the interface uses a standard serial distribution of ABINIT. However, calculations for large systems can still be performed by means of consecutive runs, which are automatically set up by the interface, with minimal input or intervention from a user.

(2) *Density components*: Fourier components of the

ground-state density $\rho(\mathbf{G})$ are generated using the eigenfunctions from stage (1).

(3) *Dipole matrix elements*: Dipole matrix elements in Eq. (8) are calculated, and the eigenfunctions are converted to the format used by NBSE.

(4) NBSE *calculation*: All quantities required for the Bethe-Salpeter calculation are collected and NBSE is run. The output includes various optical spectra and optical constants.

[1] P. Hohenberg and W. Kohn, Phys. Rev. **136**, B864 (1964).
[2] W. Kohn and L. J. Sham, Phys. Rev. **140**, A1133 (1965).
[3] M. C. Payne, M. P. Teter, D. C. Allan, T. A. Arias, and J. D. Joannopoulos, Rev. Mod. Phys. **64**, 1045 (1992).
[4] L. Hedin, Phys. Rev. **139**, A796 (1965).
[5] F. Aryasetiawan and O. Gunnarsson, Rep. Prog. Phys. **61**, 237 (1998).
[6] W. Hanke and L. J. Sham, Phys. Rev. B **12**, 4501 (1975).
[7] S. Ismail-Beigi, Phys. Status Solidi C **3**, 3365 (2006).
[8] M. Lopez del Puerto, M. L. Tiago, and J. R. Chelikowsky, Phys. Rev. Lett. **97**, 096401 (2006).
[9] M. Cardona and G. Harbeke, Phys. Rev. **137**, A1467 (1965).
[10] L. X. Benedict and E. L. Shirley, Phys. Rev. B **59**, 5441 (1999).
[11] X. Gonze *et al.*, Comput. Mater. Sci. **25**, 478 (2002).
[12] F. Sottile, K. Karlsson, L. Reining, and F. Aryasetiawan, Phys. Rev. B **68**, 205112 (2003).
[13] P. Puschnig and C. Ambrosch-Draxl, Phys. Rev. B **66**, 165105 (2002).
[14] W. G. Schmidt, S. Glutsch, P. H. Hahn, and F. Bechstedt, Phys. Rev. B **67**, 085307 (2003).
[15] G. Onida, L. Reining, and A. Rubio, Rev. Mod. Phys. **74**, 601 (2002).
[16] Z. H. Levine and S. G. Louie, Phys. Rev. B **25**, 6310 (1982).
[17] M. S. Hybertsen and S. G. Louie, Phys. Rev. B **37**, 2733 (1988).
[18] E. L. Shirley, Phys. Rev. B **54**, 16464 (1996).
[19] M. Mikami, S. Nakamura, O. Kitao, H. Arakawa, and X. Gonze, Jpn. J. Appl. Phys., Part 2 **39**, L847 (2000).
[20] E. L. Shirley, J. Electron Spectrosc. Relat. Phenom. **136**, 77 (2004).
[21] E. L. Shirley, J. A. Soininen, and J. J. Rehr, Proc. SPIE **5538**, 125 (2004).
[22] M. Rohlfing and S. G. Louie, Phys. Rev. B **62**, 4927 (2000).
[23] G. Csanak, H. S. Taylor, and R. Yaris, Adv. At. Mol. Phys. **7**, 287 (1971).
[24] L. J. Sham and T. M. Rice, Phys. Rev. **144**, 708 (1966).
[25] E. K. Chang, M. Rohlfing, and S. G. Louie, Phys. Rev. Lett. **85**, 2613 (2000).
[26] J. A. Soininen, J. J. Rehr, and E. L. Shirley, J. Phys.: Condens. Matter **15**, 2573 (2003).
[27] R. Haydock, Comput. Phys. Commun. **20**, 11 (1980).
[28] H. M. Lawler, J. J. Rehr, S. D. Dalosto, E. L. Shirley, Z. H. Levine, A. P. Sorini, and F. Vila, AI2NBSE Code and Documentation, 2008, World Wide Web, http://leonardo.phys.washington.edu/ai2nbse/.
[29] H.-C. Weissker, J. Serrano, S. Huotari, F. Bruneval, F. Sottile, G. Monaco, M. Krisch, V. Olevano, and L. Reining, Phys. Rev. Lett. **97**, 237602 (2006).
[30] R. B. Laughlin, Phys. Rev. B **22**, 3021 (1980).
[31] S. T. Pantelides and M. Long, in *Physics of* SiO_2 *and its Interfaces*, edited by S. T. Pantelides (Pergamon, New York, 1978), p. 339.
[32] R. B. Sosman, *The Properties of Silica* (Chemical Catalogue, New York, 1927).
[33] K. M. Glassford and J. R. Chelikowsky, Phys. Rev. B **46**, 1284 (1992).
[34] S. D. Mo and W. Y. Ching, Phys. Rev. B **51**, 13023 (1995).
[35] R. Asahi, Y. Taga, W. Mannstadt, and A. J. Freeman, Phys. Rev. B **61**, 7459 (2000).
[36] A. Fahmi, C. Minot, B. Silvi, and M. Caus'a, Phys. Rev. B **47**, 11717 (1993).
[37] D. Reyes-Coronado, G. Rodríguez-Gattorno, M. E. Espinosa-Pesqueira, C. Cab, R. de Coss, and G. Oskam, Nanotechnology **19**, 145605 (2008).
[38] P. I. Sorantin and K. Schwarz, Inorg. Chem. **31**, 567 (1992).
[39] N. Troullier and J. L. Martins, Phys. Rev. B **43**, 1993 (1991).
[40] M. Teter, Phys. Rev. B **48**, 5031 (1993).
[41] G. Jellison, L. A. Boatner, J. D. Budai, B.-S. Jeong, and D. P. Norton, J. Appl. Phys. **93**, 9537 (2003).
[42] D. W. Fischer, Phys. Rev. B **5**, 4219 (1972).
[43] H. R. Philipp and H. Ehrenreich, Phys. Rev. **129**, 1550 (1963).
[44] N. Hosaka, T. Sekiya, C. Satoko, and S. Kurita, J. Phys. Soc. Jpn. **66**, 877 (1997).
[45] H. Modrow, S. Bucher, J. J. Rehr, and A. L. Ankudinov, Phys. Rev. B **67**, 035123 (2003).